Relationship between Typhoons with Concentric Eyewalls and ENSO in the Western North Pacific Basin

YI-TING YANG

Office of Disaster Management, New Taipei City, Taiwan

HUNG-CHI KUO

Department of Atmospheric Sciences, National Taiwan University, Taipei, Taiwan

ERIC A. HENDRICKS

Marine Meteorology Division, Naval Research Laboratory, Monterey, California

YI-CHIN LIU

Pacific Northwest National Laboratory, Richland, Washington

MELINDA S. PENG

Marine Meteorology Division, Naval Research Laboratory, Monterey, California

(Manuscript received 29 July 2014, in final form 15 December 2014)

ABSTRACT

The typhoons with concentric eyewalls (CE) over the western North Pacific in different phases of the El Niño–Southern Oscillation (ENSO) between 1997 and 2012 are studied. They find a good correlation (0.72) between the annual CE typhoon number and the oceanic Niño index (ONI), with most of the CE typhoons occurring in the warm and neutral episodes. In the warm (neutral) episode, 55% (50%) of the typhoons possessed a CE structure. In contrast, only 25% of the typhoons possessed a CE structure in the cold episode. The CE formation frequency is also significantly different with 0.9 (0.2) CEs per month in the warm (cold) episode. There are more long-lived CE cases (CE structure maintained more than 20 h) and typhoons with multiple CE formations in the warm episodes. There are no typhoons with multiple CE formations in the cold episode. The warm episode CE typhoons generally have a larger size, stronger intensity, and smaller variation in convective activity and intensity. This may be due to the fact that the CE formation location is farther east in the warm episodes. Shifts in CE typhoon location with favorable conditions thus produce long-lived CE typhoons and multiple CE formations. The multiple CE formations may lead to expansion of the typhoon size.

1. Introduction

There have been extensive studies of tropical cyclones (TCs) in different El Niño–Southern Oscillation (ENSO) phases, and no significant correlation has been found between the annual TC genesis number and ENSO over the western North Pacific basin (e.g., Ramage and Hori 1981; Lander 1993, 1994; Chen et al. 2006). The annual genesis number, however, increases over the southeastern part of the western North Pacific and decreases over the northwestern part in El Niño (the warm episode) and a reversed situation occurred in La Niña (the cold episode) (Atkinson 1977; Chen et al. 1998; Chan 2000; Chia and Ropelewski 2002; Camargo et al. 2007; Zhan et al. 2011). In terms of TC tracks, TCs are more likely to recurve toward higher latitudes before landfall because the genesis region is farther east in the warm episode. In contrast, TCs tend to move more westward, increasing the probability of landfall over

Corresponding author address: Hung-Chi Kuo, Department of Atmospheric Sciences, National Taiwan University, No. 1, Sec. 4, Roosevelt Road, Taipei 10617, Taiwan.
E-mail: kuo@as.ntu.edu.tw

DOI: 10.1175/JCLI-D-14-00541.1

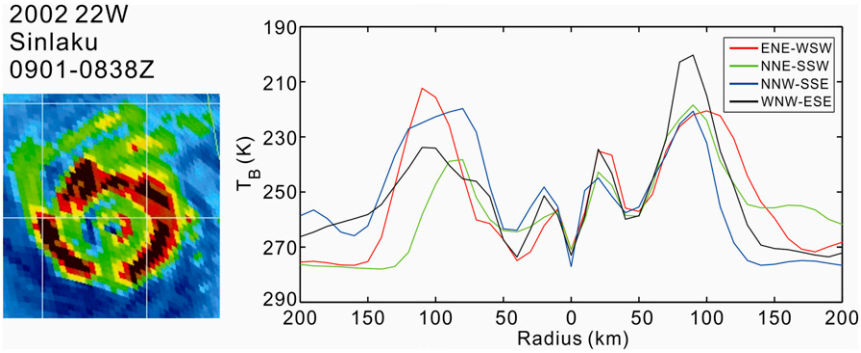

FIG. 1. Color-enhanced microwave CE imagery of Typhoon Sinlaku (2002). The averaged T_B profiles of eight radial directions for Typhoon Sinlaku are conformed to the CE-determined criteria. Note that the T_B is set to decrease upward so that a low T_B value (deep convection) is high in the coordinate.

China in the late season of cold episode years (Elsner and Liu 2003; Wu et al. 2004; Camargo et al. 2007). In addition, there are more intense and long-lived typhoons in the warm episode than in the cold episode (Chia and Ropelewski 2002; Camargo and Sobel 2005; Li and Zhou 2012). Because of the shift of the genesis region, the mean duration time of TCs over the ocean tends to be longer during the warm episode than in the cold episode (Wang and Chan 2002).

Strong TCs are often observed to have a concentric eyewall (CE) structure, with an inner eyewall and an outer eyewall separated by a convective minimum region, the moat (Willoughby et al. 1982; Hawkins and Helveston 2004). CE formation and the subsequent eyewall replacement cycle (ERC) may lead to large variability in structure and intensity changes (e.g., Willoughby et al. 1982; Black and Willoughby 1992; Kuo et al. 2009; Sitkowski et al. 2011). Yang et al. (2013) used an objective method to identify three different CE types in the western North Pacific: (i) CE with the typical inner-eyewall dissipated ERC, (ii) CE with outer-eyewall dissipated replacement cycle due to environmental vertical wind shear, and (iii) CE structure that is maintained for an extended period of more than 20 h. The cases in which the CE structure is maintained for an extended period of time often have larger sizes and exist in favorable environmental conditions.

As stated above, shifts in TC tracks and environmental conditions have been linked to phase changes in ENSO. Since the variations in the environment have been linked to variability in CE characteristics (Yang et al. 2013), the purpose of this study is to examine frequency and storm structures of CE typhoons in relation to ENSO. This is the first study to examine CE frequency in relation to ENSO. We will show that the warm phase of the oceanic Niño index is more conducive to CEs, multiple CEs per storm, and larger/longer-lived storms. Section 2 describes the data and the methodology. Section 3 addresses the CE observations in different ENSO phases. Section 4 summarizes the results.

2. Data and methodology

We use the passive Special Sensor Microwave Imager (SSM/I) and passive Tropical Rainfall Measuring Mission (TRMM) Microwave Imager (TMI) 85-GHz data (Kummerow et al. 1998) imagery. These data were obtained from the Naval Research Laboratory (NRL) Marine Meteorology Division in Monterey, California (Hawkins et al. 2001). Using the antenna gain function associated with the sampled radiometer data, the NRL microwave satellite images are reprocessed to create high-resolution (1–2 km) products that can aid in defining inner-storm structural details (Hawkins and Helveston 2004; Hawkins et al. 2006). The CE structure is identified by the objective method of Yang et al. (2013) from microwave satellite imagery between 1997 and 2012. The objective method uses mean and the standard deviation of blackbody brightness temperature (T_B) in eight radial profiles to the CE detection. The criteria ensures not just that the symmetric CE structure exists but also that the moat (high T_B value) is significant, the outer eyewall has strong deep convection (low T_B value), and the outer eyewall is not a spiral band. An image of Typhoon Sinlaku (2002) with a CE is presented in Fig. 1, along with the eight radial profiles of T_B for this case.

The storm intensity was obtained from the Joint Typhoon Warning Center (JTWC) best-track data in this study. The monthly-mean Interim European Centre for Medium-Range Weather Forecasts (ECMWF) Re-Analysis (ERA-Interim) is used for composite analyses

of TC environment conditions. The ERA-Interim data are interpolated to pressure levels for this study. The ERA-Interim dataset has a spectral T255 horizontal resolution, which is approximately 79-km horizontal resolution in physical space. This dataset (http://rda.ucar.edu/datasets/ds627.0/) is the newest global atmospheric reanalysis generated by ECMWF with an improved numerical model and four-dimensional variation data assimilation system (Dee et al. 2011).

The NCEP warm and cold episodes data are based on a threshold of ±0.5°C for the oceanic Niño index (ONI) in the Niño-3.4 region (5°N–5°S, 120°–170°W). The ONI data are a product of a 3-month running mean of sea surface temperature in the Niño-3.4 region and they are used to classify the environmental condition of CE formation (http://www.cpc.ncep.noaa.gov/products/analysis_monitoring/ensostuff/ensoyears.shtml). The Niño-3.4 sea surface temperature anomaly is used because it is better correlated with overall tropical storm activity (Wang and Chan 2002). There are 43 months for 5 warm episodes, 66 months for 6 cold episodes, and 78 months for 10 neutral episodes. Three episodes occur in almost every season.

3. Observation and analysis

Figure 2 shows the composited sea surface temperature (SST), 500-hPa specific humidity, and 200–850-hPa vertical wind shear during the warm, cold, and neutral episodes between 1997 and 2012. Figure 2a demonstrates the mean warm seawater is elongated farther to the east (west) over the western North Pacific during warm (cold) episodes than it is during neutral episodes (Figs. 2d,g). The 850-, 500-, and 200-hPa composited specific humidity fields have similar phenomena (we only show the 500-hPa specific humidity in Figs. 2b,e,h). The extent of moist air in warm and normal episodes at 500 hPa is elongated farther to the east over the western North Pacific (Figs. 2b,h) than in the cold episode (Fig. 2e). Although the moistest air is located in the western Pacific basin during cold episodes, the moist air coverage is more extensive (farther east) during the warm episodes. Figure 2c demonstrates that the weak vertical wind shear coverage during cold episodes is broader than it is during the warm episodes. However, in Fig. 2l, the vertical wind shear difference composited between warm and cold episodes also clearly shows that the weaker vertical wind shear occurs in the southeast part (0°–20°N, 150°E–180°), and stronger vertical wind shear occurs in the northwest part (20°–40°N, 120°–150°E) of the western North Pacific during warm episodes. This phenomenon is consistent with previous study of Li and Zhou (2012). They found that the weaker vertical wind shear in the southeast part of the western North Pacific provides favorable conditions for supertyphoon development during El Niño years, while unfavorable conditions in the northwest suppress the formation of tropical storms. In summary, the warm SST and high specific humidity air elongate farther east in the western North Pacific during warm episodes. In the vertical wind shear term, the weak (strong) vertical wind shear occurs in the southeast (northwest) part of western North Pacific during warm episodes.

Figure 3 gives the locations of CE formation events over the western North Pacific between 1997 and 2012. Figure 3 suggests that CE typhoons during cold (warm) episodes tend to occur farther west (east) over the western North Pacific. The eastward shift of the genesis region may be due to the warm seawater and moist air extending farther east (west) over the western North Pacific during warm (cold) episodes and the weak vertical wind shear in the southeast part of western North Pacific during warm episodes (Fig. 2). This result is consistent with the eastward shift of the TC genesis region in the warm episode (Atkinson 1977; Chen et al. 1998; Chan 2000; Chia and Ropelewski 2002; Camargo et al. 2007; Zhan et al. 2011). As seen in Figs. 2 and 3, the east (west) shift of CE formation location in warm (cold) episode occurs in different environmental conditions. The warm episode CE typhoons in general experience low vertical shear, warm SSTs, and high 500-hPa humidity conditions. Moreover, the averaged period from category 1 intensity to landfall of the CE typhoons is much longer in the warm episode than in the cold episode (Fig. 4). The time period of category 1 intensity to the first CE formation, however, is of no significant difference in all episodes. We will show that the eastward shift of CE formation location and travel for a longer period of time over favorable ocean conditions has a profound impact on the CE structures.

Figure 5 shows the typhoon number, the CE typhoon number, and the CE typhoon percentage for three episodes from 1997 to 2012. The statistical significance is calculated using the two-proportion z test. The result shows the differences between warm and cold episodes and warm and neutral episodes are statistically significant at the 99% confidence level. Figure 5 indicates that 55% (50%) of typhoons possessed CE structures in their lifetimes during warm (neutral) episodes. In contrast, only 25% of typhoons formed CE structure in the cold episodes. Table 1 shows there are 69 (65 and 102) typhoons and 38 (16 and 51) CE formation during the warm (cold and neutral) episodes between 1997 and 2012. There are on the average 1.6, 1.3, and 1.0 typhoon formations per month in the warm, neutral, and cold episodes, respectively. The monthly CE formation frequencies are 0.9, 0.7, and 0.2 in warm, neutral, and cold

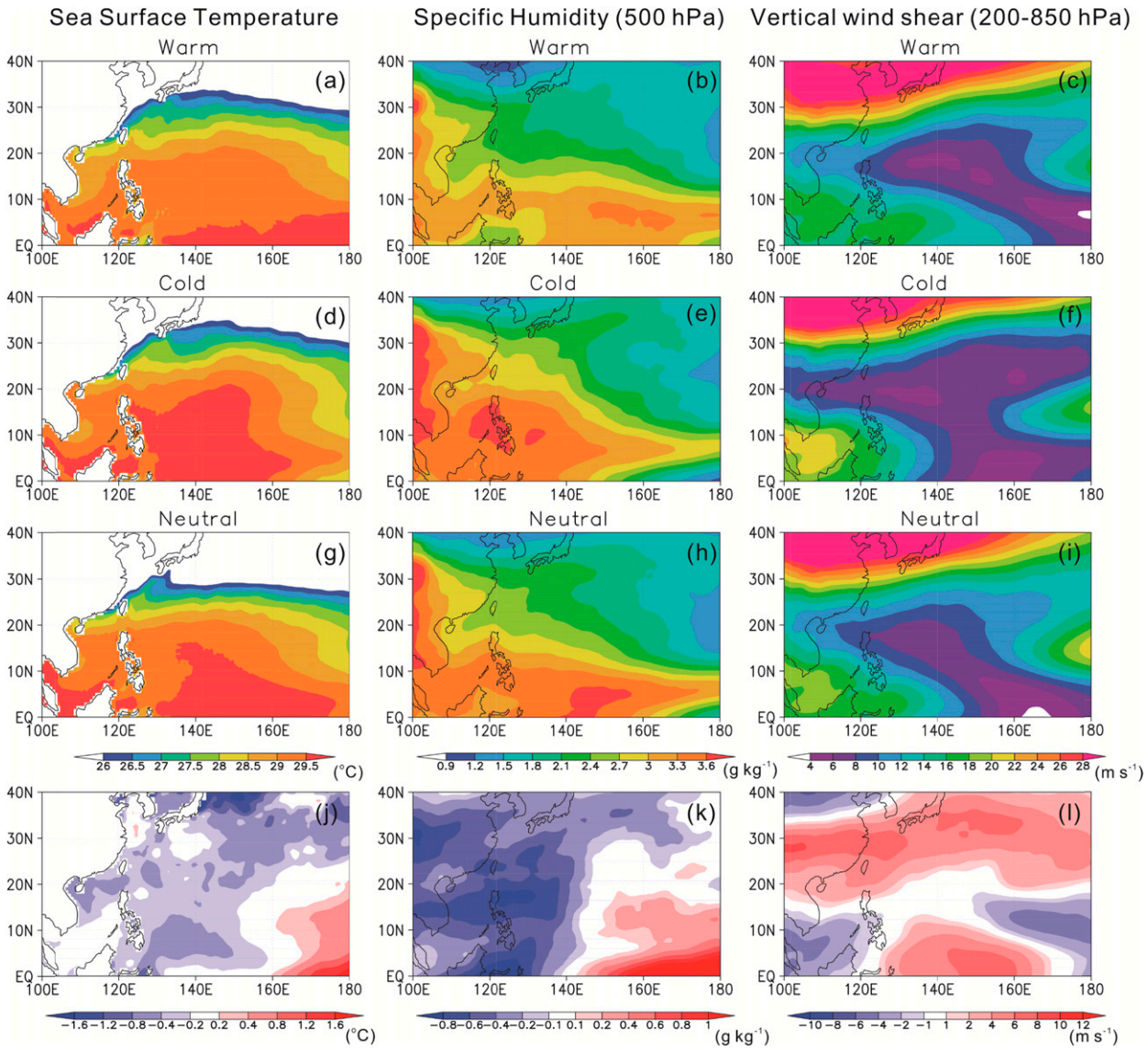

FIG. 2. (a),(d),(g) The composited sea surface temperature of warm, cold, and neutral episodes between 1997 and 2012; (b),(e),(h) the composited 500-hPa special humidity of warm, cold, and neutral episodes between 1997 and 2012, respectively; (c),(f),(i) the composited 200–850-hPa vertical wind shear of warm, cold, and neutral episodes between 1997 and 2012, respectively; and (j)–(l) the sea surface temperature, 500-hPa special humidity, and 200–850-hPa vertical wind shear difference, respectively, composited between warm and cold episodes.

episodes, respectively. The frequency of CE formation during warm episodes is 4.5 times larger than that in the cold episodes despite the fact that the frequency of TC formation in warm episodes is only 1.6 times than that in cold episodes.

Figure 6 shows the correlation of mean ONI index with annual typhoon number, strong typhoon number (the typhoons with category 4–5 intensity), CE cases, and CE typhoon number. Figure 6 indicates the correlation between annual CE typhoons number and ONI by year is 0.72, and the correlation between CE cases and ONI by year is 0.59. Figure 6b shows the correlation of annual strong typhoons and ONI is 0.65, which is consistent with previous studies (Chia and Ropelewski 2002; Camargo and Sobel 2005; Li and Zhou 2012) that show more intense typhoons occur in the El Niño phase than in the La Niña phase. All these correlations discussed are higher than the correlation of typhoon number and ONI by year (0.39). The low correlation of typhoon number and ONI have been reported in previous studies (Ramage and Hori 1981; Lander 1993, 1994; Chen et al. 2006) that there is no significant correlation between the annual TC genesis number and ENSO over western North Pacific. The better correlation of CE typhoons

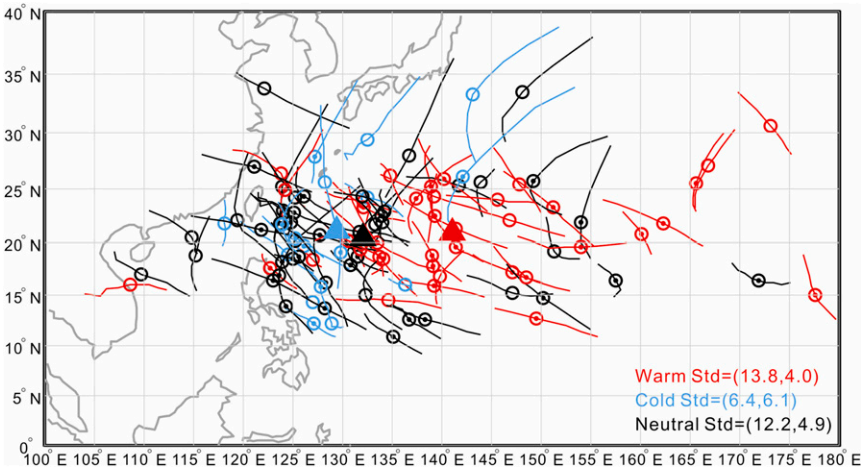

FIG. 3. Tracks within 48 h centered at CE typhoon formation in the western North Pacific from 1997 to 2012. The warm, cold, and neutral episodes are represented by red, blue, and black, respectively. The circles with (without) a dot are the locations of the CE typhoon formation with intensity greater than or equal to (less than) category 4 on the Saffir–Simpson scale. The triangle symbols represent the mean formation position of CE typhoons in each episode. The standard deviations of formation position in terms of longitude and latitude are indicated in the bottom right.

and ONI may be due to the fact that the CE structure is likely to occur in strong typhoons. The correlation was higher with CE typhoons than with CE cases may be due to the fact that second CE formation may be controlled by both internal and environmental factors.

Figure 7 shows the composited time series of intensities and normalized intensity for the CE cases formation during warm, cold, and neutral episodes as well as the average of the total CE samples. The normalized intensities of Emanuel (2000) and Knaff et al. (2003) are plotted for the comparison. The composite was computed relative to the CE formation time (for all CE cases), the maximum intensity time [for Emanuel (2000) cases], or annular hurricane formation time [for Knaff et al. (2003) cases]. The normalized intensity gives the relative change of intensity with respect to the CE formation intensity or maximum intensity. The near-landfall cases and the cases with poor satellite temporal resolution (greater than 12 h) are excluded in the analysis of Fig. 7. The near-landfall case is defined when the typhoon center was within 200 km from land in the 24-h period before or after CE formation. Figure 7a suggests that the average intensity of CE cases during the warm episode is stronger than that during cold and neutral episodes 18 h before and 24 h after CE formation. The CE storms in the cold episode have a more rapid intensification rate than that of the warm episode. Of the 10 CE cases in the cold episode, there are 9 storms with intensity change before the CE formation meet the rapidly intensifying criteria of $\Delta V_{\max} \geq 19.5\ \mathrm{m\ s^{-1}}$ in 24 h (Hendricks et al. 2010). In particular, the CE storms during warm and cold episodes still intensified continuously for 6 h after CE formation. Then, the intensity of CE storms during warm (cold) episodes decreases slowly (quickly). The quick decline of intensity during

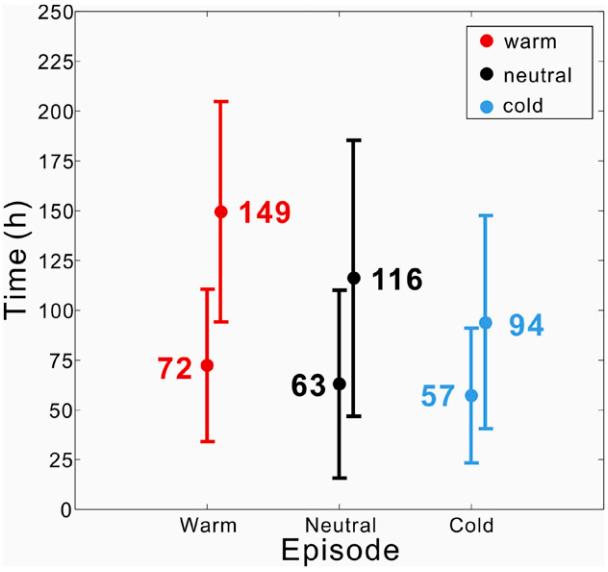

FIG. 4. The averaged time period of CE typhoons with standard deviations (left) from category 1 intensity to the first CE formation and (right) from category 1 intensity to landfall or intensity demise to tropical storm during warm (red), cold (blue), and neutral (black) episodes.

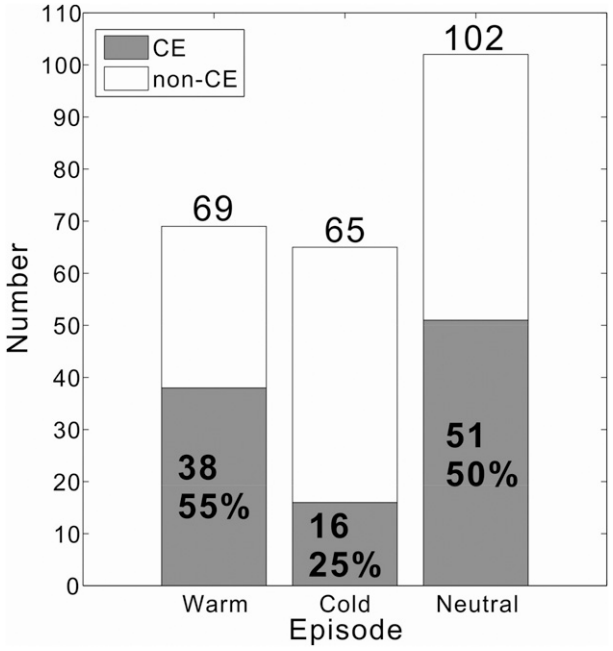

FIG. 5. Histogram of the no-CE typhoons and CE typhoons in three different episodes from 1997 to 2012. The total typhoon numbers and the CE typhoon percentages in each episode are indicated.

TABLE 1. The number of typhoons and concentric eyewall cases per month during warm, cold, and neutral episodes.

	Warm	Cold	Neutral
Typhoon number/month	69/43 = 1.6	65/66 = 1.0	102/78 = 1.3
CE cases/month	38/43 = 0.9	16/66 = 0.2	51/78 = 0.7

cold episodes is likely due to the colder SST and lower specific humidity encountered. The composited intensity tendency for CE typhoons during warm episodes prior to formation is distinctively different from the CE typhoons during cold and neutral episodes. The CE typhoons composite reaches a higher normalized intensity prior to CE formation in the warm episode. Compared to cold episodes, the intensity composite in warm episodes shows a relatively high intensity for a longer duration, rather than that in cold episodes with a substantial rapid intensification process. Kuo et al. (2004, 2008) highlighted the importance of axisymmetrization dynamics of positive vorticity perturbations around a strong and tight core of vorticity in the formation of CE structure and the core vortex with large circulation may produce larger size CE storm. The long duration of high intensity before CE formation may provide a favorable environment for the axisymmetrization dynamics to operate.

To explore the CE storm structures in the warm, cold and neutral episodes, six scatter diagrams involving the moat width (d_0), inner-eye radius (r_0), outer-eyewall width (w_0), and cyclone intensity at CE structure formation (V_{CE}) during warm, cold, and neutral episodes are plotted (Fig. 8). The mean and standard deviations of CE size during three different episodes are also shown. In general, the large scatter in these diagrams indicates no significant relationships among different structural parameters of inner-eyewall radius, moat width, outer-eyewall width, and intensity for the CE typhoon cases. The only exception is the moat width and outer-eyewall width (Fig. 8c). Figure 8c indicates that the outer-eyewall width is larger with a larger moat width ($R^2 = 0.44$). It also shows that the CE typhoons that have moat widths larger than 60 km and outer-eyewall widths larger than 80 km only form during warm and neutral episodes.

Hill and Lackmann (2009) suggested that more environmental moisture favors a larger TC size. The large size typhoon and wider outer eyewall in a warm episode may be due to the presence of more environmental moisture. On the other hand, the large moat size may be due to the vortex-scale filamentation dynamics of stronger TCs (Rozoff et al. 2006; Kuo et al. 2008, 2012). Yang et al. (2013) found that the filamentation moat width explains more than 55% of the variance of the satellite-observed moat width in the western North Pacific. While it is well known that subsidence is important in the maintenance of the CE typhoon moat, it may be that in a strong TC the subsidence is confined to the edge of the deep convection by inertial stability and is less likely to uniformly organize the moat width [analogous to the eye subsidence distribution work of Schubert et al. (2007)].

In summary, the mean CE size during warm episodes is larger than the other two episodes (Fig. 8). The intensity and convective activity (CA) changes can be demonstrated by the T–V_{max} diagram (Yang et al. 2013), a diagram in which the ordinate is CA in terms of the brightness temperature T_B contrast to the background in the 400 km by 400 km area of satellite imagery centered at the eye, and the abscissa is the best-track estimated cyclone intensity. Figure 9a shows the T–V_{max} diagrams for CE typhoons during warm, neutral, and cold episodes. The near-landfall cases and poor temporal resolution cases are excluded in this diagram. Here, the time of CE formation is marked along with 48 h before and after CE formation. Both CA and intensity could be maintained at the value 24 h before and 12 h after the CE formation and the values change slowly within the 96 h during warm episodes. The standard deviation of T_B and V during warm episode are the smallest (1.3 K and

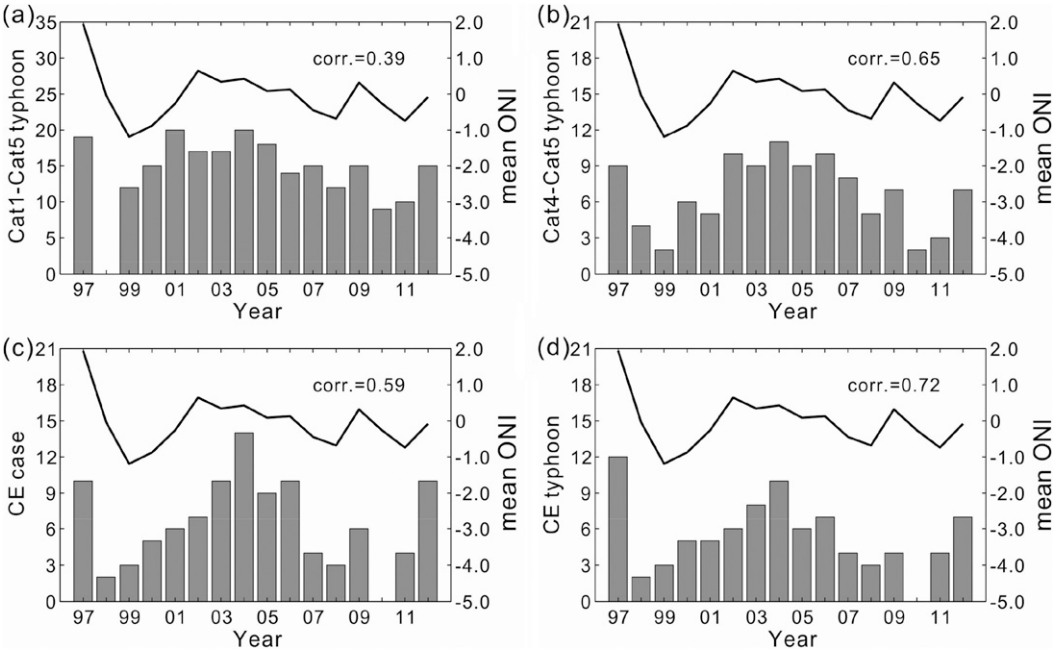

FIG. 6. Number of (a) category 1–5 typhoons, (b) category 4–5 typhoons, (c) CE cases (multiple CE formations are included), and (d) CE typhoons by years (histograms and left ordinate) and the mean ONI by year (line and right ordinate). The correlation between number and mean ONI is shown. The correlation coefficient for (b)–(d) is significant at the 99% confidence interval, while the correlation coefficient for (a) is not statistically significant (lower than 90%).

5 m s^{-1}, respectively) in all episodes. On the contrary, the intensity and CA increased (weakened) quickly 48 h before (after) CE formation during cold episode. The T–V_{max} diagram of no-CE formation typhoons with category 4 and 5 intensity during three warm, cold, and neutral episodes is shown in Fig. 9b. The CA and intensity change patterns are similar during these different episodes but with lower values than that in the CE cases.

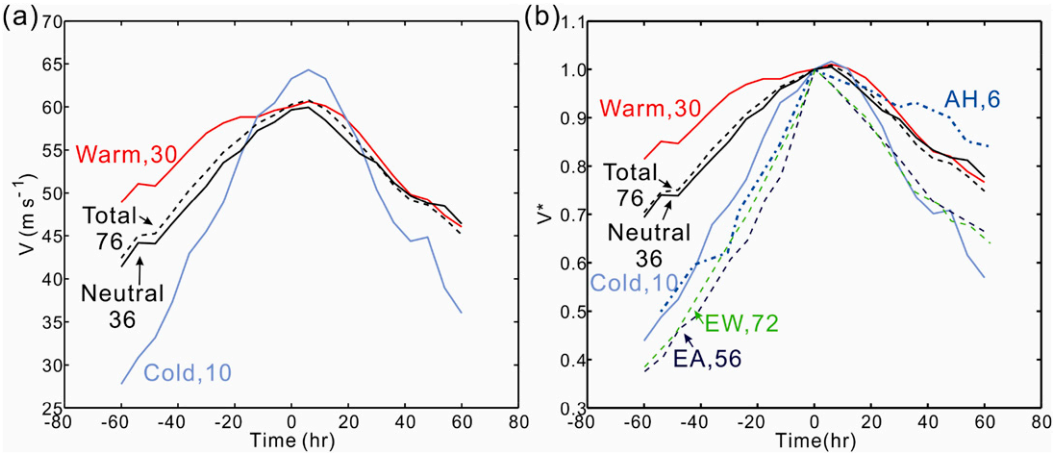

FIG. 7. Composited time series of (a) intensity and (b) normalized intensity for the CE cases during warm, cold, and neutral episodes and all CE cases. The normalized intensities associated with average tropical cyclones in the Atlantic (EA) and western North Pacific (EW) that did not encounter cold water or make landfall as report by Emanuel (2000) and annular hurricanes (AH) as reported by Knaff et al. (2003) are plotted for comparison. The composite was computed relative to CE formation time (for all CE cases), annular hurricane formation time (for Knaff et al.'s cases), or the maximum intensity time (for Emanuel's cases). The number of cases is indicated next to each line.

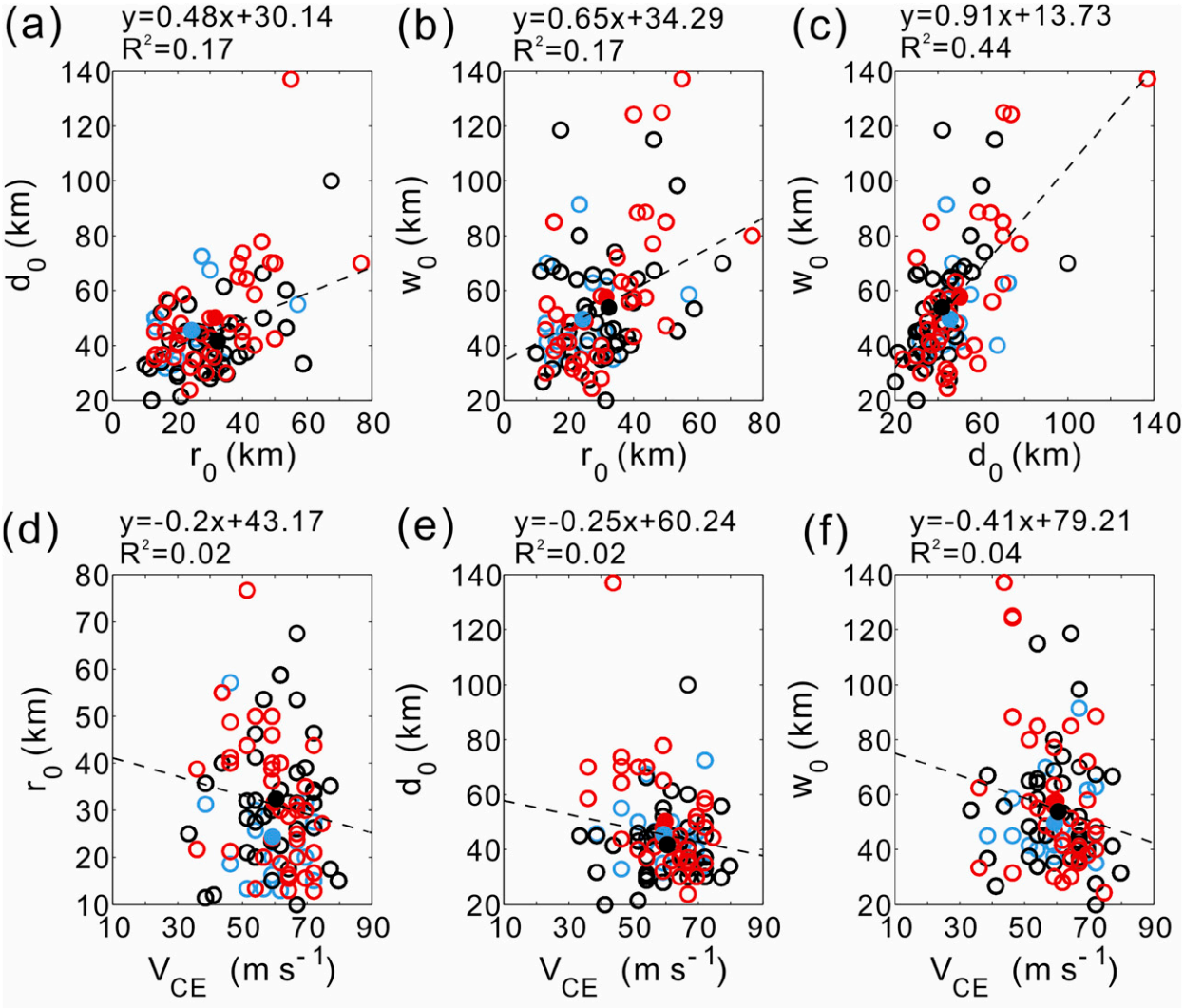

	r_0(mean,std)	d_0(mean,std)	w_0(mean,std)	size(mean,std)
Warm	31.6,14.2	50.2,20.1	57.6,27.7	139.4,54.6
Cold	24.4,11.3	45.5,11.8	49.7,15.4	119.6,27.3
Neutral	32.4,15.8	41.7,14.0	53.8,21.7	128.0,39.9

FIG. 8. Scatter diagrams of (a) moat width vs inner-eyewall radius, (b) outer-eyewall width vs inner-eyewall radius, (c) outer-eyewall width vs moat width, (d) inner-eyewall radius vs cyclone intensity, (e) moat width vs cyclone intensity, and (f) outer-eyewall width vs cyclone intensity at CE formation time. The warm, cold, and neutral episodes are represented by red, blue, and black colors, respectively. The table represents mean and standard deviation of inner-eyewall radius, moat width, and outer-eyewall width for CE cases during warm, cold, and neutral episodes (unit: km). The mean and standard deviations of CE size are also shown.

In summary, Figs. 8 and 9 indicate the mean CE size is larger, but the CA and intensity variations are smaller in the warm episode than that in other episodes.

Yang et al. (2013) identified three different CE types from microwave satellite imagery: CE with the eyewall replacement cycle where the inner eyewall dissipates and it replaced by the contracting outer eyewall (the ERC cases), CE with outer eyewall dissipated by unfavorable environmental conditions prior to the replacement cycle (the NRC cases), and CE structure that

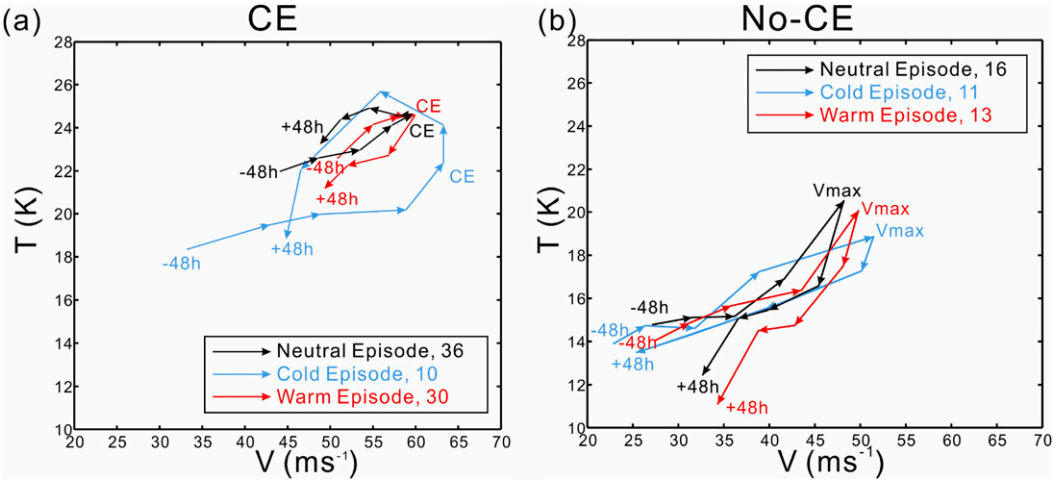

FIG. 9. The averaged T_B and cyclone intensity changes in 48 h before and after CE formation for (a) CE cases and (b) no CE cases with intensity greater than category 4 on the Saffir–Simpson scale during warm, cold, and neutral episodes. Case numbers are given in figures. Each arrow is in the 12-h time interval.

is maintained for an extended period of more than 20 h (the CEM cases). In the time period of 1997–2012, we find that the CEM, NRC, and ERC cases are 18, 19, and 39, respectively. Table 2 indicates 50% (47% and 31%) of CEM (NRC and ERC) cases formed during warm episodes, 17% (5% and 15%) of CEM (NRC and ERC) cases formed during cold episodes, and 33% (47% and 54%) of CEM (NRC and ERC) cases formed during neutral episodes. Previous studies indicate that there are more intense and long-lived typhoons in the El Niño phase than in the La Niña phase (Chia and Ropelewski 2002; Camargo and Sobel 2005; Li and Zhou 2012). There are only three CEM cases with 20–29-h duration, and there are no CEM cases with duration greater than or equal to 30 h during cold episode (Fig. 10). Consistent with the more intense and long-lived typhoons in the warm episode, our results suggest that the long-lived CEM cases also tend to occur in the warm episode.

Table 3 shows that multiple CE formations (with second or third CE formations) cases per month are also higher in the warm episode: 0.37 compared to 0.29 in the neutral episode. There are no multiple CE cases in the cold episode. Tables 2 and 3 suggest that the long-lived CE TCs and multiple CE formations are favored in the warm episode. It may be because the CE typhoons in the warm episodes tend to occur farther east over the western North Pacific and with more favorable environmental conditions (SST, specific humidity, and vertical wind shear). The long-lived CE structures and multiple CE formations in warm episode may be due to the TCs' long journey over the ocean.

Finally, we note that the expansion of the averaged structural parameters in the multiple CE (MCE) formations cases (Fig. 11). We also include the structural

TABLE 2. The number and percentage of CEM, NRC, ERC, and landing or no data cases during warm, cold, and neutral episodes.

Episode	CEM (18)	NRC (19)	ERC (39)	Landing or no data (29)
Warm	9 (50%)	9 (47%)	12 (31%)	8 (28%)
Cold	3 (17%)	1 (5%)	6 (15%)	6 (21%)
Neutral	6 (33%)	9 (47%)	21 (54%)	15 (52%)

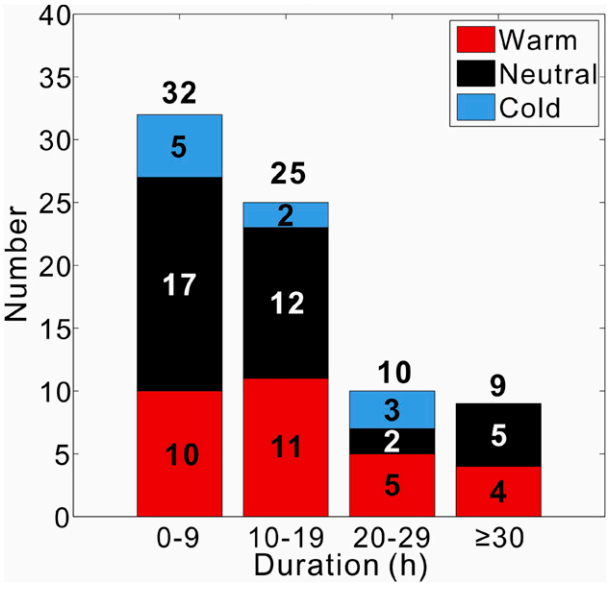

FIG. 10. The number of CE cases in different episodes as a function of duration time in the western North Pacific basin between 1997 and 2012. The number of CE cases in each episode is indicated. The near-landfall cases are excluded.

TABLE 3. The multiple concentric eyewall cases per month during warm, cold, and neutral episodes.

Episode	Multiple CE cases/month
Warm	16/43 = 0.37
Cold	0/66 = 0
Neutral	23/78 = 0.29

parameters in the single (SCE) CE formation cases and total CE (TCE) cases in Fig. 11. The structural parameters in the first CE formation are of no distinct difference either in SCE and MCE cases or in each different episode. On the other hand, the CE size expands in the multiple formations. The multiple CE formation process is the reason for the large size parameters in the warm episode. As an example of CE typhoon in warm episode, Typhoon Winnie (1997) is the largest typhoon in the western North Pacific (Zhang et al. 2005). Typhoon Winnie (1997) had two CE periods with 20- and 46.5-h duration times. The 46.5-h duration is the longest CE duration record in the western North Pacific. The inner-eyewall radius, moat width, and outer-eyewall width of Typhoon Winnie (1997) were 17 (55), 57 (137), and 40 (137) km in the first (second) CE formation. There is significant expansion of all size parameters in the multiple CE process in Typhoon Winnie.

4. Conclusions

The relationship between concentric eyewall (CE) typhoons and different ENSO phases has been examined. The CE typhoons are identified with an objective method from microwave satellite image between 1997 and 2012. The NCEP oceanic Niño index (ONI) warm and cold episode data are used to classify the environmental conditions of CE typhoons formation. Since the shift in typhoon tracks has been linked to phase changes in ENSO, the CE formation rate and the structures could also be distinct in different ENSO phases. In the warm episode, the mean location of CE formation is farther east over the western North Pacific and the long journey over warm ocean with weaker vertical shear makes the CE typhoons differ from those in the cold episode. The primary findings are that the warm phase

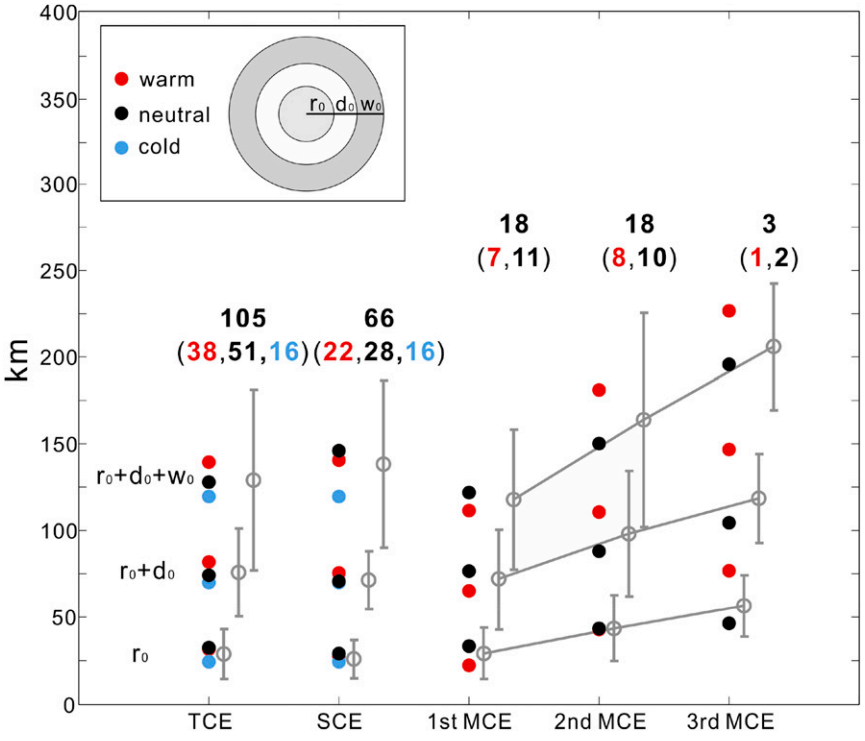

FIG. 11. The mean and standard deviation of r_0, $r_0 + d_0$, and $r_0 + d_0 + w_0$ of total CE cases; single CE formation cases; and the first, second, and third multiple CE formations cases. The gray lines are average values and standard deviations. The means of r_0, $r_0 + d_0$, $r_0 + d_0 + w_0$, and number during warm (red dot), cold (blue dot) and neutral (black dot) episodes are shown. The gray lines are slightly shifted for clarity. The r_0, d_0, and w_0 are the inner-eyewall radius, moat width, and outer-eyewall width, respectively.

of the ONI is more conducive to CEs, multiple CEs per storm, and larger/longer-lived storms. Our results are as follows:

1) A very good relationship of 0.72 was found between the annual CE typhoon number with the ONI, with most of the CE typhoons occurring in the warm and neutral episodes.
2) There are 55% (50%) of the typhoons that possessed CE structures in the warm episode (neutral episode). In contrast, only 25% of the typhoons in the cold episode possessed CE structures. The averaged CE formation frequency is significantly different, with 0.9 (0.2) per month in the warm (cold) episode.
3) There are more long-lived CE cases (CE structure maintained more than 20 h) and multiple CE formations in the warm episodes. The cold episode CE typhoons do not have multiple CE formations.
4) The warm episode CE typhoons have larger size, stronger intensity, and smaller variation in convective activity and intensity changes in the eyewall replacement process.
5) The structural parameters in the first CE formation are of no distinct difference either in SCE and MCE cases or in each different episode. Multiple CE formation, on the other hand, leads to significant size expansion in CE typhoons.

Acknowledgments. This research is sponsored by Ministry of Science and Technology, Taiwan, under Grants MOST 103-2111-M-002-010, MOST 103-2625-M-002-003, MOST 100-2111-M-002-004-MY3, and NTU-CESRP-103R7604-1 and by the U.S. Office of Naval Research NICOP Grant N62909-11-1-7096. We appreciate the comments of the three anomalous reviewers; their reviews helped us to improve the manuscript greatly.

REFERENCES

Atkinson, G. D., 1977: Proposed system for near real time monitoring of global tropical circulation and weather patterns. *Proc. 11th Tech. Conf. on Hurricanes and Tropical Meteorology,* Miami Beach, FL, Amer. Meteor. Soc., 645–652.

Black, M. L., and H. E. Willoughby, 1992: The concentric eyewall cycle of Hurricane Gilbert. *Mon. Wea. Rev.,* **120,** 947–957, doi:10.1175/1520-0493(1992)120<0947:TCECOH>2.0.CO;2.

Camargo, S. J., and A. H. Sobel, 2005: Western North Pacific tropical cyclone intensity and ENSO. *J. Climate,* **18,** 2996–3006, doi:10.1175/JCLI3457.1.

——, K. A. Emanuel, and A. H. Sobel, 2007: Use of a genesis potential index to diagnose ENSO effects on tropical cyclone genesis. *J. Climate,* **20,** 4819–4834, doi:10.1175/JCLI4282.1.

Chan, J. C. L., 2000: Tropical cyclone activity over the western North Pacific associated with El Niño and La Niña events. *J. Climate,* **13,** 2960–2972, doi:10.1175/1520-0442(2000)013<2960:TCAOTW>2.0.CO;2.

Chen, T. C., S. P. Weng, N. Yamazaki, and S. Kiehne, 1998: Interannual variation in the tropical cyclone activity over the western North Pacific. *Mon. Wea. Rev.,* **126,** 1080–1090, doi:10.1175/1520-0493(1998)126<1080:IVITTC>2.0.CO;2.

——, S. Y. Wang, and M. C. Yen, 2006: Interannual variation of tropical cyclone activity over the western North Pacific. *J. Climate,* **19,** 5709–5720, doi:10.1175/JCLI3934.1.

Chia, H.-H., and C. F. Ropelewski, 2002: The interannual variability in the genesis location of tropical cyclones and the northwest Pacific. *J. Climate,* **15,** 2934–2944, doi:10.1175/1520-0442(2002)015<2934:TIVITG>2.0.CO;2.

Dee, D. P., and Coauthors, 2011: The ERA-Interim reanalysis: Configuration and performance of the data assimilation system. *Quart. J. Roy. Meteor. Soc.,* **137,** 553–597, doi:10.1002/qj.828.

Elsner, J. B., and K. B. Liu, 2003: Examining the ENSO-typhoon hypothesis. *Climate Res.,* **25,** 43–54, doi:10.3354/cr025043.

Emanuel, K., 2000: A statistical analysis of tropical cyclone intensity. *Mon. Wea. Rev.,* **128,** 1139–1152, doi:10.1175/1520-0493(2000)128<1139:ASAOTC>2.0.CO;2.

Hawkins, J. D., and M. Helveston, 2004: Tropical cyclone multiple eyewall characteristics. *26th Conf. on Hurricane and Tropical Meteorology,* Miami, FL, Amer. Meteor. Soc., P1.7. [Available online at https://ams.confex.com/ams/pdfpapers/76084.pdf.]

——, T. F. Lee, F. J. Turk, C. Sampson, J. Kent, and K. Richardson, 2001: Real-time Internet distribution of satellite products for tropical cyclone reconnaissance. *Bull. Amer. Meteor. Soc.,* **82,** 567–578, doi:10.1175/1520-0477(2001)082<0567:RIDOSP>2.3.CO;2.

——, M. Helveston, T. F. Lee, F. J. Turk, K. Richardson, C. Sampson, J. Kent, and R. Wade, 2006: Tropical cyclone multiple eyewall characteristics. Preprints, *27th Conf. on Hurricane and Tropical Meteorology,* Monterey, CA, Amer. Meteor. Soc., 6B.1. [Available online at https://ams.confex.com/ams/pdfpapers/108864.pdf.]

Hendricks, E. A., M. S. Peng, B. Fu, and T. Li, 2010: Quantifying environmental control on tropical cyclone intensity change. *Mon. Wea. Rev.,* **138,** 3243–3271, doi:10.1175/2010MWR3185.1.

Hill, K. A., and G. M. Lackmann, 2009: Influence of environmental humidity on tropical cyclone size. *Mon. Wea. Rev.,* **137,** 3294–3315, doi:10.1175/2009MWR2679.1.

Knaff, J. A., J. P. Kossin, and M. DeMaria, 2003: Annular hurricanes. *Wea. Forecasting,* **18,** 204–223, doi:10.1175/1520-0434(2003)018<0204:AH>2.0.CO;2.

Kummerow, C., W. Barnes, T. Kozu, J. Shiue, and J. Simpson, 1998: The Tropical Rainfall Measuring Mission (TRMM) sensor package. *J. Atmos. Oceanic Technol.,* **15,** 809–817, doi:10.1175/1520-0426(1998)015<0809:TTRMMT>2.0.CO;2.

Kuo, H.-C., L.-Y. Lin, C.-P. Chang, and R. T. Williams, 2004: The formation of concentric vorticity structures in typhoons. *J. Atmos. Sci.,* **61,** 2722–2734, doi:10.1175/JAS3286.1.

——, W. H. Schubert, C.-L. Tsai, and Y.-F. Kuo, 2008: Vortex interactions and barotropic aspects of concentric eyewall formation. *Mon. Wea. Rev.,* **136,** 5183–5198, doi:10.1175/2008MWR2378.1.

——, C.-P. Chang, Y.-T. Yang, and H.-J. Jiang, 2009: Western North Pacific typhoons with concentric eyewalls. *Mon. Wea. Rev.,* **137,** 3758–3770, doi:10.1175/2009MWR2850.1.

——, ——, and C.-H. Liu, 2012: Convection and rapid filamentation in Typhoon Sinlaku during TCS-08/T-PARC. *Mon. Wea. Rev.,* **140,** 2806–2817, doi:10.1175/MWR-D-11-00314.1.

Lander, M. A., 1993: Comments on "A GCM simulation of the relationship between tropical storm formation and ENSO." *Mon. Wea. Rev.,* **121,** 2137–2143, doi:10.1175/1520-0493(1993)121<2137:COGSOT>2.0.CO;2.

——, 1994: An exploratory analysis of the relationship between tropical storm formation in the western North Pacific and ENSO. *Mon. Wea. Rev.,* **122,** 636–651, doi:10.1175/1520-0493(1994)122<0636:AEAOTR>2.0.CO;2.

Li, R. C. Y., and W. Zhou, 2012: Changes in western Pacific tropical cyclones associated with the El Niño–Southern Oscillation cycle. *J. Climate,* **25,** 5864–5878, doi:10.1175/JCLI-D-11-00430.1.

Ramage, C. S., and A. M. Hori, 1981: Meteorological aspects of El Niño. *Mon. Wea. Rev.,* **109,** 1827–1835, doi:10.1175/1520-0493(1981)109<1827:MAOEN>2.0.CO;2.

Rozoff, C. M., W. H. Schubert, B. D. McNoldy, and J. P. Kossin, 2006: Rapid filamentation zones in intense tropical cyclones. *J. Atmos. Sci.,* **63,** 325–340, doi:10.1175/JAS3595.1.

Schubert, W. H., C. M. Rozoff, J. L. Vigh, B. D. McNoldy, and J. P. Kossin, 2007: On the distribution of subsidence in the hurricane eye. *Quart. J. Roy. Meteor. Soc.,* **133,** 595–605, doi:10.1002/qj.49.

Sitkowski, M., J. P. Kossin, and C. M. Rozoff, 2011: Intensity and structure changes during hurricane eyewall replacement cycles. *Mon. Wea. Rev.,* **139,** 3829–3847, doi:10.1175/MWR-D-11-00034.1.

Wang, B., and J. C. L. Chan, 2002: How strong ENSO events affect tropical storm activity over the western North Pacific. *J. Climate,* **15,** 1643–1658, doi:10.1175/1520-0442(2002)015<1643:HSEEAT>2.0.CO;2.

Willoughby, H. E., J. A. Clos, and M. G. Shoreibah, 1982: Concentric eye walls, secondary wind maxima, and the evolution of the hurricane vortex. *J. Atmos. Sci.,* **39,** 395–411, doi:10.1175/1520-0469(1982)039<0395:CEWSWM>2.0.CO;2.

Wu, M. C., W. L. Chang, and W. M. Leung, 2004: Impact of El Niño–Southern Oscillation events on tropical cyclone landfalling activity in the western North Pacific. *J. Climate,* **17,** 1419–1428, doi:10.1175/1520-0442(2004)017<1419:IOENOE>2.0.CO;2.

Yang, Y.-T., H.-C. Kuo, E. A. Hendricks, and M. S. Peng, 2013: Structural and intensity changes of concentric eyewall typhoons in the western North Pacific basin. *Mon. Wea. Rev.,* **141,** 2632–2648, doi:10.1175/MWR-D-12-00251.1.

Zhan, R., Y. Wang, and X. Lei, 2011: Contributions of ENSO and east Indian Ocean SSTA to the interannual variability of northwest Pacific tropical cyclone frequency. *J. Climate,* **24,** 509–521, doi:10.1175/2010JCLI3808.1.

Zhang, Q.-H., S.-J. Chen, Y.-H. Kuo, K.-H. Lau, and R. A. Anthes, 2005: Numerical study of a typhoon with a large eye: Model simulation and verification. *Mon. Wea. Rev.,* **133,** 725–742, doi:10.1175/MWR2867.1.